View metadata, citation and similar papers at core.ac.uk
brought to you by CORE
provided by Archivio istituzionale della ricerca - Università degli Studi di Udine



# On the adequacy of the Transmission Line Model to describe the graphene–metal contact resistance

Stefano Venica*, Francesco Driussi*, Gahoi Amit†‡, Pierpaolo Palestri*, Max C. Lemme†‡§ and Luca Selmi*

***Abstract*—The contact–end–resistance method is applied to TLM structures to characterize in–depth the graphene–metal contact and its dependence on the back–gate bias. Parameters describing the graphene–metal stack resistance are extracted through the widely used transmission line model. The results show inconsistencies which highlight application limits of the model underlying the extraction method. These limits are attributed to the additional resistance associated to the $p$–$p^+$ junction located at the contact edge, that is not part of the conventional transmission line model. Useful guidelines for a correct application of the extraction technique are provided, identifying the bias range in which this additional resistance is negligible. Finally, the contact–end–resistance method and the transmission line model are exploited to characterize graphene–metal contacts featuring different metals.**

***Index Terms*—Graphene Field Effect Transistor, Transfer Length Method, transmission line model, Contact–End–Resistance method**

## I. Introduction

TWO–dimentional (2D) materials (e.g. graphene and transition metal dichalcogenides) represent a very promising option for the post–silicon era in Radio–Frequency (RF) electronics [1], [2], [3], [4], [5]. Indeed, the improved electrostatic control and the large carrier mobility offered by these materials may boost the RF performance of ultimately scaled devices. However, despite the remarkable breakthroughs in 2D materials' technology in the recent years, when it comes to the fabrication of complete devices a few bottlenecks remain unsolved, which prevent attaining high performance and THz operation. In particular, one of the most stringent technological limitations comes from **the interfacial resistance between 2D materials and metals [6], [7]**. As an example, the large measured contact resistance is recognized as an important drawback for the Field Effect Transistors (FETs) based on 2D channel materials, like the Graphene-FET (GFET), that is nowadays the most mature 2D based device. Indeed, if the electrical contacts to graphene were transparent, it has been predicted that the achievable cut–off frequency of a GFET with 10 nm of channel length could be as high as 7 THz [8]. Furthermore, the contact resistance largely reduces the GFET transconductance, thus degrading the device performance [3], [9], [10]. Also other alternative device concepts based on the 2D technology suffer from the detrimental effect of the 2D material–metal contact resistance [11], [12], [13], [14].

Unfortunately, the physical mechanisms occurring at the 2D material–metal interface and contributing to the contact resistance are not well understood yet. Hence, reliable characterization techniques are essential to devise novel strategies to lower the series resistances in 2D based devices [15], [16], targeting values comparable to those of conventional and well–established technologies and meeting the ITRS requirements for series resistance in future electronics [5], [17], [18], [19].

In this framework, we characterize in–depth the graphene–metal contact. In particular, we made use of the Contact–End–Resistance (CER) method applied to Transfer Length Method (TLM) structures [20], that has been successfully used in the past to investigate metal contacts to Si and III–V compounds [20], [21]. More recently, this characterization technique has been applied to graphene based devices [22], [23], [24] and combined with the transmission line model to interpret the results. However, although this latter model is widely used to investigate the contact resistance in semiconductors, a critical analysis of our experimental data on graphene–metal contacts reveals inconsistencies and points out to often overlooked limitations in the validity of this model to describe the transition between a graphene channel and a metal contact [24]. In this paper, we assess the application range of the transmission line model for the description of the 2D material–metal contacts; furthermore, we extended the work of [24] **considering also Au–graphene contacts and by extracting the different contributions to the** contact resistance between graphene and different metals and providing insight on the dependence of the contact parameters on the metal itself.

## II. Test structures and measurement method

Figure 1 sketches the layout (a) and the corresponding cross section (b) of the measured TLM structures, that are based on a CVD monolayer graphene grown by chemical vapor deposition on copper foil by Moorfield rapid thermal processing tool and later transferred on top of 85 nm of $SiO_2$ substrate by electrochemical delamination method [25]. The complete device features a series of nine contacts plus two additional contacts at the end of the same graphene stripe. It can be seen as a sequence of ten back–gated GFETs with different channel lengths and the same channel width connected in series **[see Fig. 1(c)]. TLM structures has been**

Manuscript received ...

* Universitá degli Studi di Udine, Dipartimento Politecnico di Ingegneria e Architettura (DPIA), via delle Scienze 206, 33100 Udine, Italy (email: venica.stefano@spes.uniud.it).
† University of Siegen, School of Science and Technology, Hölderlinstr. 3, 57076 Siegen, Germany.
‡ RWTH Aachen University, Faculty of Electrical Engineering and Information Technology, Chair for Electronic Devices, Otto–Blumenthal–Str. 2, 52074 Aachen, Germany.
§ AMO GmbH, Advanced Microelectronic Center Aachen, Otto–Blumenthal–Str. 25, 52074 Aachen, Germany.

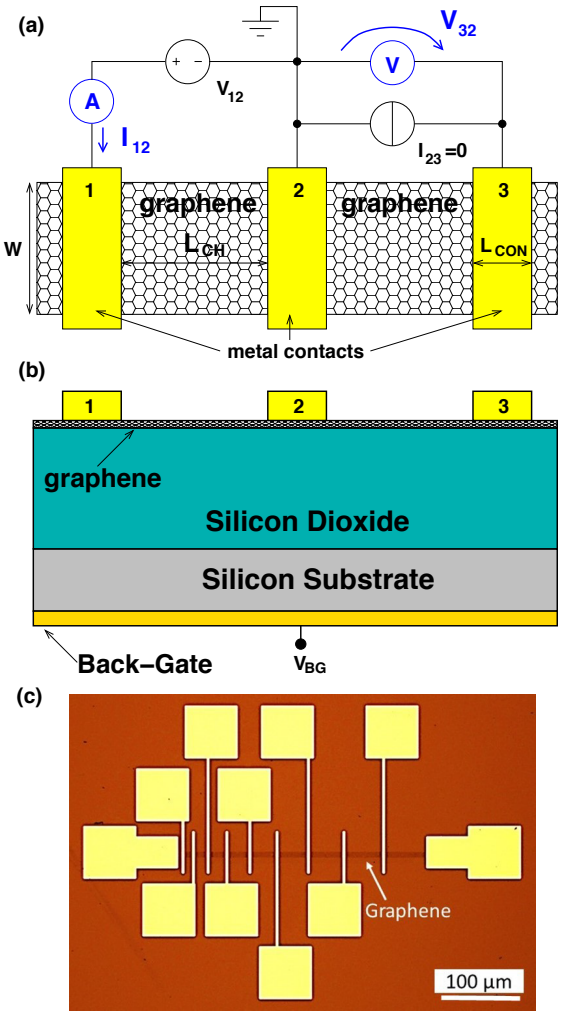


Fig. 1. (a) Layout of the TLM structure and measurement setup used for the application of the CER method. (b) Cross section of the back–gated GFETs constituting the TLM structure. $V_{BG}$ is the back–gate bias. **(c) Microscope image of a complete TLM structure. Yellow pads are the metal contacts, while the dark horizontal line is the graphene stripe. In this structure, W=5 $\mu$m, while the shortest device (left side) and the longest one (right side) measure 5 $\mu$m and 50 $\mu$m, respectively.**

**fabricated with two lithography mask sets: in the first, the spacing ($L_{CH}$) between the contacts ranges from 5 $\mu$m to 50 $\mu$m with a 5 $\mu$m increase between adjacent GFETs, while, in the second, $L_{CH}$ varies from 8 $\mu$m to 80 $\mu$m with 8 $\mu$m steps.** TLM structures with channel width [$W$, see Fig. 1(a)] varying between 4 $\mu$m and 40 $\mu$m have been measured. Unless otherwise stated, the electrical characterization on TLM structures were carried out in ambient atmosphere **(temperature 300 K and relative humidity of 21 %)**.

Figure 1(a) reports the measurement setup used to characterize the graphene–metal contact resistance. In the experiments, we apply a voltage $V_{12}$ between contact 1 and 2 and we measure the current $I_{12}$ in the GFET. In this way, we determine the total resistance $R_T$ of the device as:

$$R_T = \frac{V_{12}}{I_{12}}, \tag{1}$$

that is contributed by the sheet resistance of the graphene channel ($R_{SH}$) and by the contact–front resistance ($R_{CF}$)

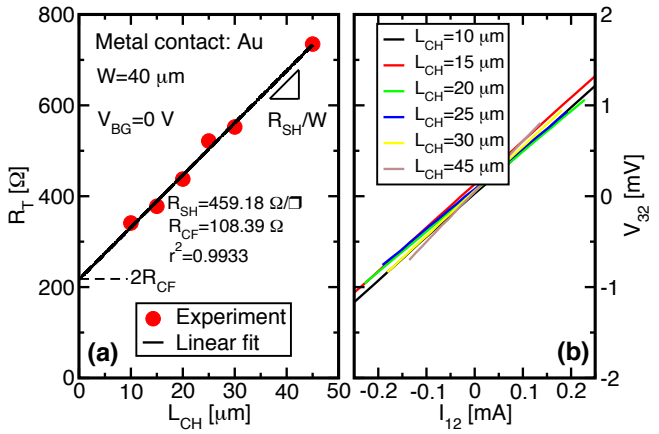


Fig. 2. (a) Total resistance as a function of $L_{CH}$ for a TLM structure with gold contacts measured at $V_{BG}$=0 V. $R_{SH}$ is extracted from the slope of the linear fit, while $R_{CF}$ is obtained from the intercept with the $y$–axis. (b) Potential drop across the graphene–Au contact as a function of $I_{12}$. The linear trend validates Eq. 3. $V_{32}$ is independent on $L_{CH}$.

related to the graphene-metal stack, namely

$$R_T = \frac{L_{CH}}{W} R_{SH} + 2R_{CF}. \tag{2}$$

Therefore, after measuring $R_T$ for devices with different channel lengths, it is possible to extract $R_{SH}$ and $R_{CF}$ through the linear fit of the $R_T$ versus $L_{CH}$ data; in particular, the $R_{SH}$ is extracted from the slope of the linear plot, while $R_{CF}$ is obtained from the intercept with the $y$–axis **[20]**. As an example, Fig. 2(a) reports the $R_T$ values measured on a TLM structure with gold contacts, showing the extraction procedure for $R_{SH}$ and $R_{CF}$.

Furthermore, during the $I_{12}$ measurement, the experimental setup of Fig. 1(a) allows to measure also the potential $V_{32}$ by imposing a null current between the contacts 2 and 3 ($I_{23}$=0). We assume that $V_{32}$ drops across the graphene–metal stack **at the end of the contact number 2 (where the current is least, Fig. 3)**. Hence, with this three–contacts setup, it is possible to obtain the so called contact–end resistance $R_{CE}$ [20], calculated as

$$R_{CE} = \frac{V_{32}}{I_{12}}, \tag{3}$$

where $I_{12}$ and $V_{32}$ are measured at the same time at the contacts 1 and 3, respectively. In this respect, in [24], we verified that the concurrent measurement of $V_{32}$ is not affecting the $I_{12}$ value. **We also check that the back–gate leakage current is negligible (in the order of pA/$\mu$m, not shown) and does not influence the measure of both $I_{12}$ and $V_{32}$.** Fig. 2(b) shows $V_{32}$ as a function of $I_{12}$ for the same TLM structure in Fig. 2(a) and the observed linear trend validates the definition of $R_{CE}$ in Eq. 3. It is worth noting that $R_{CE}$ is independent of $L_{CH}$, which confirms that $R_{CE}$ is determined only by the graphene–metal contact and it is not affected by the graphene channel.

Following [20], the contact resistance can be modeled by means of a distributed R–R transmission line model, as shown in Fig. 3 that sketches the TLM structure in proximity of the contact 2. **The resistance of the metal is neglected**

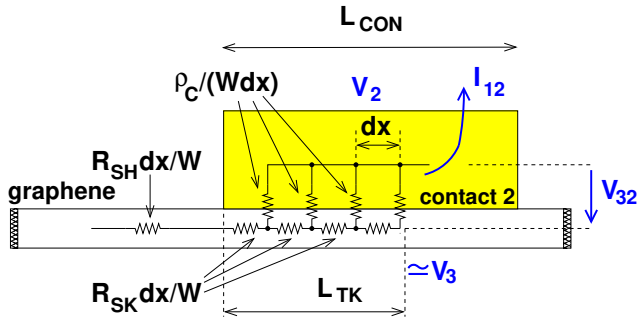


Fig. 3. Distributed R–R network constituting the transmission line model used to describe the graphene–metal contact. $\rho_C$, $R_{SK}$ and $L_{TK}$ are the model parameters. $L_{CON}$ is the contact length defined by the mask layout.

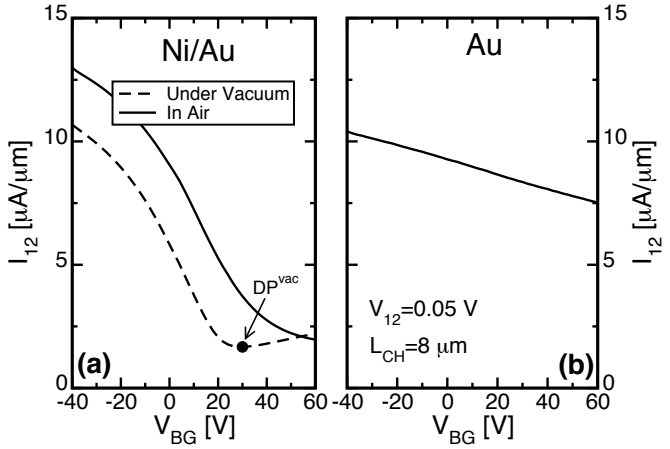


Fig. 4. Transfer characteristics of GFETs with contacts made of a Ni/Au stack (a) and Au (b). Solid lines are measurements made in air and, for both test structures, the Dirac Point (DP) is not visible in the explored $V_{BG}$ range. The dashed line is the measurement done under vacuum.

**since the large carrier concentration.** Under this assumption, the potential profile under the contact is determined by the specific contact resistivity ($\rho_C$, associated to the graphene–metal interface) and the sheet resistance of the graphene under the metal contact ($R_{SK}$). The transfer length $L_{TK}$ represents, instead, the active portion of the contact involved in the conduction and it is typically smaller than the contact length ($L_{CON}$=6 $\mu$m in our samples). Hence, it is possible to correlate the experimental $R_{CF}$ and $R_{CE}$ to the model parameter $\rho_C$, $R_{SK}$ and $L_{TK}$ through the following equations [20]:

$$R_{CE} = \frac{\rho_C}{L_{TK} W \sinh\left(\frac{L_{CON}}{L_{TK}}\right)}, \quad (4)$$

$$\frac{R_{CF}}{R_{CE}} = \cosh\left(\frac{L_{CON}}{L_{TK}}\right), \quad (5)$$

$$L_{TK} = \sqrt{\rho_C / R_{SK}}. \quad (6)$$

**Therefore, by measuring the TLM structures with the three-points setup in Fig. 1(a) and by resorting to the transmission line model above, it is possible to decouple the different contributions to $R_{CF}$, hence the horizontal graphene sheet resistivitiy under the metal ($R_{SK}$) and the vertical interfacial resistivity ($\rho_C$).**

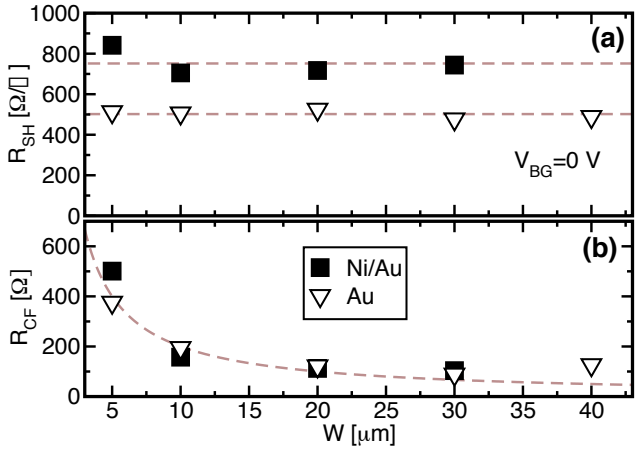


Fig. 5. **Sheet resistance (a) and contact–front resistance (b) as a function of $W$ for the Ni/Au stack (squares) and gold (triangles) contacts. For a given $W$, the data are averaged over several TLM structures. The measurements are taken at $V_{BG}$=0 V. As expected $R_{SH}$ is almost constant, while $R_{CF}$ scales inversely with $W$. Dashed lines are guides for the eyes.**

## III. Experimental results

We measured samples exploiting **Au contacts and a stack made of Ni/Au (with the Ni directly evaporated in contact with the graphene layer)**. It is worth noting that these metals have work functions higher than the affinity of graphene [26]. Consequently, the graphene under the contact should be $p$–doped [27], [28].

**We measured the samples with small $V_{12}$=0.05–0.1 V, to operate the GFETs in linear region and to guarantee uniform charge density along the graphene channel.** Figure 4 shows the transfer characteristics of two GFETs with the Ni/Au stack (a) and Au (b) as contacts. When measured in air (solid lines), in both cases, the minimum conductivity point (Dirac Point, DP) is barely visible in the explored range of the back–gate voltage ($V_{BG}$). This is the effect of the air/humidity, that strongly influences the graphene charge of the exposed channel and shifts the DP to large $V_{BG}$ values, finally resulting in heavily $p$–doped graphene [29], [30]. This interpretation is confirmed by the dashed line in Fig. 4(a), that is the experiment under vacuum, showing a DP (around 30 V) that is lower than the measurement in air (DP>60 V). Anyway, also under vacuum ($\approx 10^{-3}$ mbar), DP is not zero (as should be for undoped graphene) maybe because of the residual air/humidity or because the samples underwent a rapid thermal annealing at 450 °C, that typically shifts the DP towards positive values [31], [32]. Thus, similarly to the graphene under the contact, also the channel is $p$–doped in the explored $V_{BG}$ range. **It is also worth noting that the Au sample has the DP at a much larger $V_{BG}$ value with respect to the Ni/Au case.**

**As a first step of our study, we verified the consistency and significance of the measurements. To avoid device degradation, in the following we limit the $V_{BG}$ range to $\pm$40 V.** Figure 5 shows the graphene sheet resistance $R_{SH}$ (a) and the contact–front resistance $R_{CF}$ (b) measured at $V_{BG}$=0 V as a function of the channel width $W$, **for the Ni/Au stack (squares) and gold (triangles) contacts. As expected,**

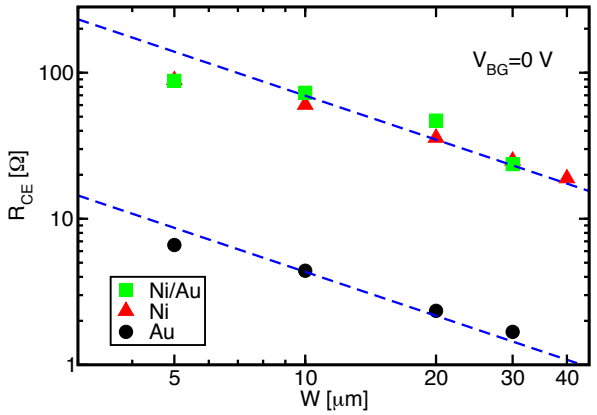


Fig. 6. Contact–end resistance versus $W$ for TLM structures with different metals. $R_{CE}$ scales inversely with $W$. Dashed lines are guides for the eyes. $R_{CE}$ is averaged over different TLM structures.

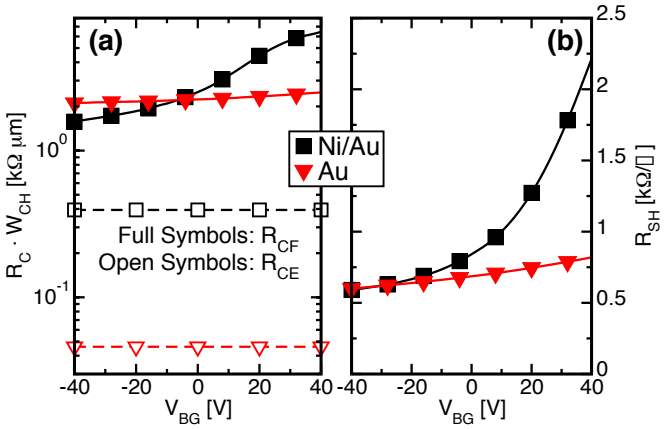


Fig. 7. Contact–front resistance (a, full symbols) and sheet resistance (b) as a function of $V_{BG}$ for the Ni/Au stack (squares) and Au (triangles) contacts. The flatter curves obtained for gold reflect the trend of the transfer characteristics in Fig. 4(b). $R_{CE}$ [open symbols in plot (a)] is independent of $V_{BG}$, suggesting a fixed potential profile under the contact.

$R_{SH}$ **is rather constant in both cases, confirming a uniform graphene quality over the samples. The slightly different** $R_{SH}$ **values when comparing the different metals reflect the different Dirac Point position in the characteristics of Fig. 4, that induces, for fixed** $V_{BG}$**, a different charge density in the channel of the two samples. The** $R_{CF}$ **is, instead, inversely proportional to** $W$**, going as** $1/W$ **[Fig. 5(b)]. For this bias (**$V_{BG}$=0 $V$**),** $R_{CF}$ **is similar for the two contacts. Finally,** also the contact–end resistance $R_{CE}$ scales inversely with $W$ as expected (see Fig. 6, note the logarithmic scales). **In this respect, Fig. 6 compares the values of** $R_{CE}$ **for the metal contacts used in this work. It is evident that** Au contacts show smaller $R_{CE}$ values than Ni/Au ones. **In [24], we also found that the** $R_{CE}$ **measured in pure Ni contacts is very similar to the one obtained for the Ni/Au stack (Ni in contact with graphene). These two facts clearly point out the smaller potential drop (**$V_{32}$**) across the Au–graphene interface than for the Ni–graphene case. Note that** $V_{32}$ **and thus** $R_{CE}$ **reflect the importance of the different contributions to** $R_{CF}$**, namely the** $R_{SK}$ **and** $\rho_C$ **values.**

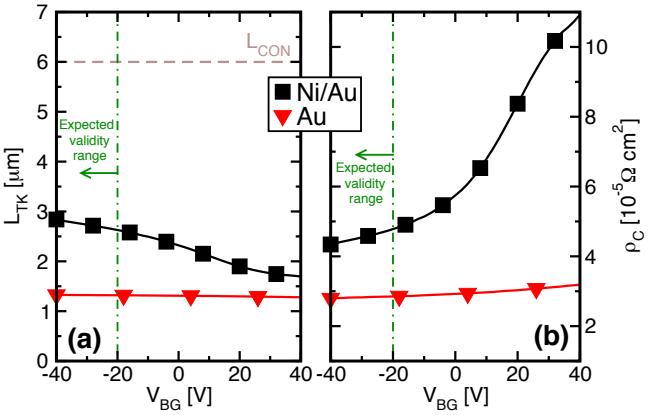


Fig. 8. Transfer length (a) and specific contact resistivity (b) extracted by solving Eqs. 4–6, in case of the Ni/Au stack (squares) and Au (triangles) contacts. For the Ni/Au stack, in spite of the rather constant $R_{CE}$ in Fig. 7, $L_{TK}$ and $\rho_C$ largely vary with $V_{BG}$, following the $R_{CF}$ trend. This suggests limits in the applicability range of the transmission line model within this experimental framework.

**Having assessed the consistency of the experimental data set, we studied the dependence of measurements on the back–gate biasing.** Figure 7 shows that both $R_{CF}$ (a) and $R_{SH}$ (b) increase with increasing $V_{BG}$, with a stronger dependence in the case of the Ni/Au stack with respect to the Au contacts, as expected from the different transfer characteristics of the GFETs with the two metals in Fig. 4. Indeed, the $V_{BG}$ dependence of $R_{SH}$ is strictly linked to the $I_{12}$–$V_{BG}$ characteristic and the DP position; when approaching the Dirac Point, the hole density ($p_{CH}$) in the graphene channel drops, thus increasing its resistivity, since

$$R_{SH} = (q\mu_P p_{CH})^{-1}, \tag{7}$$

where $\mu_P$ is the graphene hole mobility and $q$ is the elementary charge [12]. **Far away from the DP (**$V_{BG}$<−20 **V), **$R_{SH}$ **is similar for both the samples, indicating similar graphene quality.**

**In constrast to the** $R_{CF}$ **strongly depending on** $V_{BG}$**, Fig. 7(a) reports also the corresponding measured** $R_{CE}$ **values (open symbols), that is constant over the whole range of** $V_{BG}$**, similarly to what reported in [22], [23], [24]. This constant trend** suggests that the potential profile under the contact is rather independent of the applied $V_{BG}$ and, consequently, the hole density in the graphene under the contact is constant and fixed by the electro–chemical interactions between the graphene and the metal (Fermi level pinning in the graphene in contact with the metal) [28]. **This picture is widely accepted in the literature [19], [28], [33], [34], [35], although some authors conclude in a depinning of the Fermi level, basically due to the lack of screening of the back–gate [36], [37].** If the metal fixes the charge in the underneath graphene, the components of the R–R network constituting the transmission line ($\rho_C$ and $R_{SK}$ in Fig. 3) are expected to be constant as a function of $V_{BG}$.

By solving Eqs. 4–6 with the data of Fig. 7(a), we calculate $L_{TK}$ and $\rho_C$ for Au contacts (Fig. 8, triangles) and for the Ni/Au stack (squares). For gold, the extracted parameters are almost constant in the whole $V_{BG}$ range, as expected since

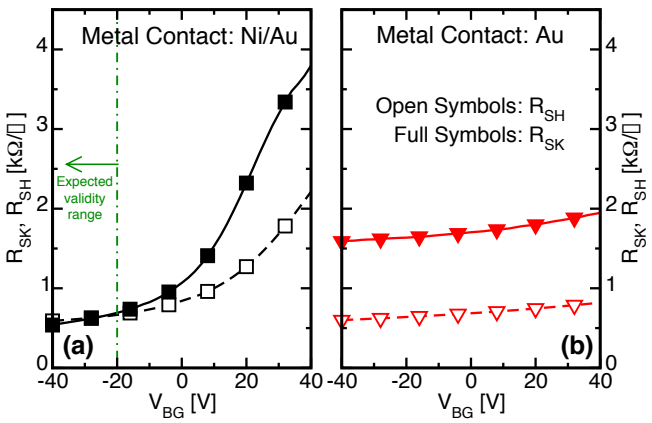


Fig. 9. Sheet resistance under the contact (full symbols) and in the channel (open symbols) for the Ni/Au stack (a) and the Au contact (b).

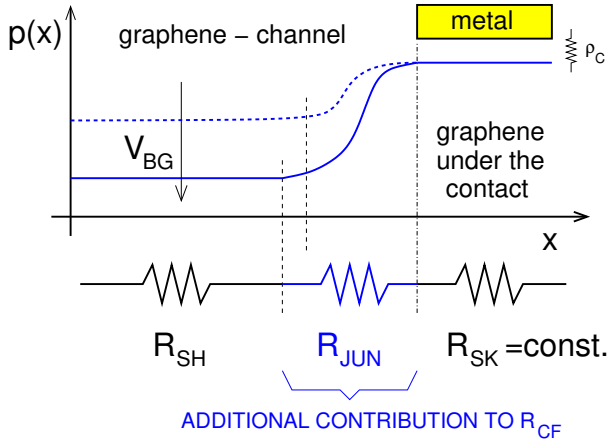


Fig. 10. Sketch of the hole density profile along the graphene in proximity of the contact edge. The step between the channel and the region under the contact (higher at large $V_{BG}$) lead to a $p$–$p^+$ junction. The associated junction resistance $R_{JUN}$ is not included in the transmission line model and it can impact the extracted graphene–metal contact parameters.

the $R_{CF}$–$V_{BG}$ curve in Fig. 7(a) (filled triangles) is almost flat. For the Ni/Au stack instead, $L_{TK}$ and $\rho_C$ tend to be constant only for $V_{BG}<-20$ V, while they strongly vary for $V_{BG}>-20$ V, hence when approaching the DP. This is due to the large $R_{CF}$ increase with $V_{BG}$ seen in Fig. 7(a) (filled squares), **that leads to a $L_{TK}$ varying with $V_{BG}$ (see Eq. 5; $R_{CE}$ is constant).**

A similar behavior (for both metals) is shown also by the extracted $R_{SK}$: indeed, in Fig. 9(b), the sheet resistance underneath the Au contact (full symbols) is weakly dependent on $V_{BG}$, similarly to the measured $R_{SH}$ trend (open symbols). Instead, for the Ni/Au stack in Fig. 9(a), only at $V_{BG}<-20$ V $R_{SK}$ changes weakly with $V_{BG}$ (with a value very close to the extracted $R_{SH}$), while for $V_{BG}>-20$ V, $R_{SK}$ strongly increases with $V_{BG}$. This large $R_{SK}$ modulation in Fig. 9(a) raises questions on the validity of the extracted parameters. In fact, it suggests a large change of the hole density in the graphene under the Ni/Au contact, but this is in contrast with the Fermi level pinning in the graphene suggested by the constant $R_{CE}$ in Fig. 7(a) and discussed above. **In other words, if the metal contact is expected to set the doping in the underneath graphene, the $R_{SK}$ modulation with $V_{BG}$ cannot be explained and appears as a limitation of the simple R–R model.** Furthermore, the $R_{SK}$ increase with $V_{BG}$ in Fig. 9(a) (filled squares) is even larger than the increase of $R_{SH}$ with $V_{BG}$ (open squares), suggesting that the modulation with $V_{BG}$ of the hole density in the graphene under the contact is stronger than in the graphene channel. This behavior is particularly difficult to be explained, since the $V_{BG}$ dependence of the graphene charge under the contact should be mitigated by the influence of the metal. Similar results are reported (but not discussed in details) also in [22], [23].

## IV. Discussion

The anomalous trend of $R_{SK}$ in Fig. 9 emerges under specific bias conditions ($V_{BG}>-20$ V) and suggests the failure of the transmission line model to describe the graphene–metal contact (at least in these experimental environment). A possible explanation is related to different hole concentrations in the graphene channel and in the region underneath the metal that may form a $p$–$p^+$ pseudo–junction located at the contact edge (see the sketch in Fig. 10). This $p$–$p^+$ step can be associated to an additional "junction" resistance $R_{JUN}$ that depends on $V_{BG}$, since at least the hole density in the channel is modulated by the back–gate bias [15], [24], [38]. Indeed, $R_{JUN}$ is not included in the transmission line model, since it is located outside the contact, but contributes to the series resistance in the GFET. Hence, by neglecting the $R_{JUN}$ contribution and by applying directly the transmission line model to the $R_{CF}$ and $R_{CE}$ results, it is possible to generate unintentional artifacts in the extracted parameters.

$R_{JUN}$ can be correctly neglected only if the $p$–$p^+$ step is rather small, hence the hole density in the graphene channel is close to that under the contact. Indeed, at $V_{BG}<-20$ V, the Ni/Au sample has a large hole density in the channel, as revealed by the small $R_{SH}$ values in Fig. 9(a). In particular, by assuming the same hole mobility in the channel and under the contact, since $R_{SH}$ and $R_{SK}$ are almost equal, the graphene charge should be very similar in the two regions. Hence the $p$–$p^+$ junction vanishes, leading to a null $R_{JUN}$. So, under this bias condition, the transmission line model correctly describes the contact and the extracted $R_{SK}$, $L_{TK}$ and $\rho_C$ are reliable.

For $V_{BG}>-20$ V, instead, we are approaching the Dirac Point, thus decreasing the hole concentration in the channel [as confirmed by the increase of $R_{SH}$ in Fig. 9(a)]. By assuming that the metal is anyway inducing a large hole concentration in the graphene under the contact, the $p$–$p^+$ junction appears (see the solid line in Fig. 10) and $R_{JUN}$ increases with $V_{BG}$, becoming non negligible. Under this bias condition, the transmission line model is not sufficient to describe the contact resistance since it does not consider all the contributions to $R_{CF}$, thus making the extraction method not reliable. Indeed, we end up in $R_{SK}$ values that show a $V_{BG}$ dependence larger than that of $R_{SH}$. Above findings lead to unreliable extraction of $\rho_C$ and $L_{TK}$.

This reasoning allows us to assume an approximate range of validity for the extraction technique **based on the transmission line model**, that we evidenced with a green arrow in

Figs. 8 and 9(a) for the Ni/Au case. For the gold contacts, instead, since measurements are far from the DP (see Fig. 4), hence the graphene channel is strongly $p$–doped, $R_{JUN}$ is always negligible and the extracted parameters are reliable in the whole explored $V_{BG}$ range.

**Note that, $R_{CF}$ and $R_{SH}$ are, instead, extracted directly from the TLM structures relying on a constant charge density in the whole channel of the GFETs. Of course, the presence of a junction in proximity of the contact edge can modify the charge profile near the source and drain and, hence, can affect the $R_{CF}$ and $R_{SH}$ values. However, it has been reported that the extension of such junctions is much smaller of our GFET lenghts [9], [38], [39], making negligible the non uniformity near the contacts and the extracted values valid in the whole $V_{BG}$ range.**

Once the validity range of the method was assessed, we compared the parameter extracted for the two contact types. Fig. 9 shows that graphene underneath the Au contact exhibits larger sheet resistance ($R_{SK}\simeq$1.7 k$\Omega/\square$) than under the Ni/Au stack ($R_{SK}\simeq$0.6 k$\Omega/\square$). This result suggests a limited capability of the Au metallisation to induce charge in the graphene; hence a weaker interaction between graphene and gold with respect to graphene and nickel. This is in line with the fact that graphene has a weak binding (physisorption) with gold, while it is chemisorbed by the nickel [28].

The above results agree with the smaller $R_{CE}$ measured for gold than for nickel in Fig. 7(a). In fact, the larger the $R_{SK}$ value is, the larger the voltage drop on this component of the R–R network will be, thus reducing the voltage drop on the graphene–metal interface ($V_{32}$).

Finally, within the assumed range of validity ($V_{BG}<-20$ V), Ni/Au shows larger $L_{TK}$ [Fig. 8(a)] than Au, with just a modest increase in $\rho_C$ [Fig. 8(b)]. This indicates better contact properties for the graphene–Ni stack than for the graphene–Au one, as confirmed by the smaller $R_{CF}$ in Fig. 7(a) [16]. **Nevertheless, because of the tight link between $R_{SK}$ and $R_{CF}$ inferable from the the comparison of Figs. 7 and 9, the improvement of the graphene quality, that improves $\mu_P$ and reduces $R_{SK}$ (see Eq. 7), would be beneficial to the $R_{CF}$ value as well, independently of the metal used for contacts.**

## V. Conclusion

We used the CER method to investigate the graphene–metal contact resistance, that we interpret through the transmission line model. The widespread use of this latter to study the semiconductor–metal contacts should be taken with caution in view of the anomalous trends exhibited by the extracted parameters under certain bias condition. These trends suggest limits of the trasmission line model to describe adequately the graphene–metal contact resistance. In particular, we attribute the observed artifacts to the additional contribution to $R_{CF}$ of the $p$–$p^+$ junction appearing in graphene in the proximity of the contact edge. The associated junction resistance $R_{JUN}$ becomes non negligible at large $V_{BG}$ values or, more in general, when approaching the graphene DP. We believe that, under these bias conditions, $R_{JUN}$ dominates the $V_{BG}$ dependence of $R_{CF}$, making the parameter extraction method unreliable. **Hence, accounting for this additional $R_{JUN}$ contribution may help reconciling the $R_{CE}$ and $R_{CF}$ trends versus $V_{BG}$ that seem to suggest a weak metal-graphene interaction, contrarily to the expectation of a significant electrostatic doping of the graphene by the metal [28].**

We identify a $V_{BG}$ range in which $R_{JUN}$ is negligible and, consequently, the extracted parameters are reliable. **Hence, in this range, the experimental procedure discussed so far can be a reliable tool to study the nature of the metal–graphene contacts.** The measurements highlight the different hole density induced by the metals in the underlying graphene, leading to lower $R_{SK}$ that correspond to lower $R_{CF}$. This result supports the fact that electrically doping the graphene through the metals is beneficial for the electrical properties of graphene–metal stacks and provides useful insight for the optimization of the graphene contact resistance.

## Acknowledgment

The authors would like to thank Melkamu Belete, Himadri Pandey and Vikram Passi for fruitful discussions. The work was partially funded by the EU through the FP7-ICT STREP Project "GRADE" under the grant 317839 via the IU.NET consortium and through an ERC starting grant (InteGraDe, 307311). **Authors from University of Udine gratefully acknowledge EverBeing Int'l Corp. for supporting their nanoelectronics laboratory with the donation of a fully equipped probe station.**

## References

[1] M. C. Lemme, L.–J. Li, T. Palacios and F. Schwierz, "Two–Dimensional Materials for Electronic Applications", *MRS Bulletin*, vol. 39, no. 8, pp. 711–718, Aug. 2014, DOI:10.1557/mrs.2014.138.

[2] G. Fiori, F. Bonaccorso, G. Iannaccone, T. Palacios, D. Neumaier, A. Seabaugh, S. K. Banerjee and L. Colombo, "Electronics Based on Two–Dimensional Materials", *Nature Nanotechnology*, vol. 9, pp. 768–769, Oct. 2014, DOI: 10.1038/nnano.2014.207.

[3] F. Schwierz, J. Pezoldt and R. Granzner, "Two–Dimensional Materials and Their Prospects in Transistor Electronics", *Nanoscale*, vol. 7, pp. 8261–8283, Apr. 2015, DOI: 10.1039/C5NR01052G.

[4] Z. Geng, W. Kinberger, R. Granzner, J. Pezoldt and F. Schwierz, "2D Electronics – Opportunities and Limitations", *46th European Solid–State Device Research Conference (ESSDERC)*, pp. 230–235, 2016, DOI: 10.1109/ESSDERC.2016.7599628.

[5] **Y. Wu, X. Zou, M. Sun, Z. Cao, X. Wang, S. Huo, J. Zhou, Y. Yang, X. Yu, Y. Kong, G. Yu, L. Liao and T. Chen, "200 GHz Maximum Oscillation Frequency in CVD Graphene Radio Frequency Transistors", *ACS Applied Materials & Interfaces*, vol. 8, no. 39, pp. 25645–25649, Sep. 2016, DOI: 10.1021/acsami.6b05791.**

[6] A. Allain, J. Kang, K. Banerjee and A. Kis, "Electrical Contacts to Two–Dimensional Semiconductors", *Nature Materials*, vol. 14, pp. 1195–1205, Nov. 2015, DOI: 10.1038/nmat4452.

[7] Y. Xu, C. Cheng, S. Du, J. Yang, B. Yu, J. Luo, W. Yin, E. Li, S. Dong, P. Ye and X. Duan, "Contacts Between Two– and Three–Dimensional Materials: Ohmic, Schottky, and p-n Heterojunctions", *ACS Nano*, vol. 10, no. 5, pp. 4895–4919, Apr. 2016, DOI: 10.1021/acsnano.6b01842.

[8] I. Imperiale, S. Bonsignore, A. Gnudi, E. Gnani, S. Reggiani and G. Baccarani, "Computational Study of Graphene Nanoribbon FETs for RF Applications", *International Electron Devices Meeting (IEDM)*, pp. 32.3.1–32.3.4, 2010, DOI: 10.1109/IEDM.2010.5703463.

[9] A. Paussa, G. Fiori, P. Palestri, M. Geromel, D. Esseni, G. Iannaccone and L. Selmi, "Simulation of the Performance of Graphene FETs with a Semiclassical Model, Including Band–to–Band Tunneling", *IEEE Transactions on Electron Devices*, vol. 61, no. 5, pp. 1567–1574, May. 2014, DOI: 10.1109/TED.2014.2307914.

[10] T. Cusati, G. Fiori, A. Gahoi, V. Passi, M. C. Lemme, A. Fortunelli and G. Iannaccone, "Electrical Properties of Graphene–Metal Contacts", *Scientific Reports*, vol. 7, p. 5109, Jul. 2017, DOI: 10.1038/s41598-017-05069-7.

[11] H. Yang, J. Heo, S. Park, H. J. Song, D. H. Seo, K.–E. Byun, P. Kim, I. Yoo, H.–J. Chung and K. Kim, "Graphene Barristor, a Triode Device with a Gate–Controlled Schottky Barrier", *Science*, vol. 336, pp. 1140–1143, Jun. 2012, DOI: 10.1126/science.1220527.

[12] S. Venica, F. Driussi, P. Palestri, D. Esseni, S. Vaziri and L. Selmi, "Simulation of DC and RF Performance of the Graphene Base Transistor", *IEEE Transactions on Electron Devices*, vol. 61, no. 7, pp. 2570–2576, Jun. 2014, DOI: 10.1109/TED.2014.2325613.

[13] S. Vaziri, A. D. Smith, M. Östling, G. Lupina, J. Dabrowski, G. Lippert, W. Mehr, F. Driussi, S. Venica, V. Di Lecce, A. Gnudi, M. König, G. Ruhl, M. Belete and M. C. Lemme, "Going Ballistic: Graphene Hot Electron Transistors", *Solid State Communications*, vol. 224, pp. 64–75, Sep. 2015, DOI: 10.1016/j.ssc.2015.08.012.

[14] Y.–W. Lan, C. M. Torres, X. Zhu, H. Qasem, J. R. Adleman, M. B. Lerner, S.–H. Tsai, Y. Shi, L.–J. Li, W.–K. Yeh and K. L. Wang, "Dual–Mode Operation of 2D Material–Base Hot Electron Transistors", *Scientific Reports*, vol. 6, p. 32503, Sep. 2016, DOI: 10.1038/srep32503.

[15] D. Berdebes, T. Low, Y. Sui, J. Appenzeller and M. S. Lundstrom, "Substrate Gating of Contact Resistance in Graphene Transistors", *IEEE Transactions on Electron Devices*, vol. 58, no. 11, pp. 3925–3932, Nov. 2011, DOI: 10.1109/TED.2011.2163800.

[16] A. Gahoi, S. Wagner, A. Bablich, S. Kataria, V. Passi and M. C. Lemme, "Contact Resistance Study of Various Metal Electrodes with CVD Graphene", *Solid–State Electronics*, vol. 125, pp. 234–239, Nov. 2016, DOI: 10.1016/j.sse.2016.07.008.

[17] A. Meersha, H. B. Variar, K. Bhardwaj, A. Mishra, S. Raghavan, N. Bhat and M. Shrivastava, "Record Low Metal–(CVD) Graphene Contact Resistance Using Atomic Orbital Overlap Engineering", *International Electron Devices Meeting (IEDM)*, pp. 5.3.1–5.3.4, 2016, DOI: 10.1109/IEDM.2016.7838352.

[18] A. Gahoi, S. Kataria and M. C. Lemme, "Temperature Dependence of Contact Resistance for Gold–Graphene Contacts", *47th European Solid–State Device Research Conference (ESSDERC)*, pp. 110–113, 2017, DOI: 10.1109/ESSDERC.2017.8066604.

[19] **N. F. W. Thissen, R. H. J. Vervuurt, A. J. M. Mackus, J. J. L. Mulders, J.–W. Weber, W. M. M. Kessels and A. A. Bol, "Graphene Devices with Bottom–Up Contacts by Area–Selective Atomic Layer Deposition", *2D Materials*, vol. 4, no. 2, p. 025046, Mar. 2017, DOI:10.1088/2053-1583/aa636a.**

[20] G. K. Reeves and H. B. Harrison, "Obtaining the Specific Contact Resistance from Transmission Line Model Measurements", *IEEE Electron Device Letters*, vol. 3, no. 5, pp. 111–113, May 1982, DOI: 10.1109/EDL.1982.25502.

[21] M. Hajlasz, J. J. T. M. Donkers, S. J. Sque, S. B. S. Heil, D. J. Gravesteijn, F. J. R. Rietveld and J. Schmitz, "Sheet Resistance Under Ohmic Contacts to AlGaN/GaN Heterostructures", *Applied Physics Letters*, vol. 104, no. 24, p. 242109, Jun. 2014, DOI: 10.1063/1.4884416.

[22] S. Wang, D. Mao, A. Muhammad, S. Peng, D. Zhang, J. Shi and Z. Jin, "Characterization of the Quality of Metal–Graphene Contact with Contact End Resistance Measurement", *Applied Physics A*, vol. 122, no. 7, p. 643, Jul. 2016, DOI: 10.1007/s0033.

[23] S. Peng, Z. Jin, D. Zhang, J. Shi, Y. Zhang and G. Yu, "Evidence of Electric Field–Tunable Tunneling Probability in Graphene and Metal Contact", *Nanoscale*, vol. 9, pp. 9520–9528, Jun. 2017, DOI: 10.1039/c7nr02502e.

[24] S. Venica, F. Driussi, A. Gahoi, V. Passi, P. Palestri, M. C. Lemme and L. Selmi, "Detailed Characterization and Critical Discussion of Series Resistance in Graphene–Metal Contacts", *International Conference of Microelectronic Test Structures (ICMTS)*, pp. 27–31, 2017, DOI: 10.1109/ICMTS.2017.7954259.

[25] Y. Wang, Y. Zheng, X. Xu, E. Dubuisson, Q. Bao, J. Lu and K. P. Loh, "Electrochemical Delamination of CVD–Grown Graphene Film: Toward the Recyclable Use of Copper Catalyst", *ACS Nano*, vol. 5, no. 12, pp. 9927–9933, Oct. 2011, 10.1021/nn203700w.

[26] H. B. Michaelson, "The Work Function of the Elements and its Periodicity", *Journal of Applied Physics*, vol. 48, no. 11, pp. 4729–4733, Nov. 1977, DOI: 10.1063/1.323539.

[27] S. Venica, M. Zanato, F. Driussi, P. Palestri and L. Selmi, "Modeling Electrostatic Doping and Series Resistance in Graphene–FETs", *International Conference on Simulation of Semiconductor Processes and Devices (SISPAD)*, pp. 357–360, 2016, DOI: 10.1109/SISPAD.2016.7605220.

[28] G. Giovannetti, P. A. Khomyakov, G. Brocks, V. M. Karpan, J. van den Brink and P. J. Kelly, "Doping Graphene with Metal Contacts", *Physical Review Letters*, vol. 101, p. 026803, Jul. 2008, DOI: 10.1103/PhysRevLett.101.026803.

[29] A. D. Smith, K. Elgammal, F. Niklaus, A. Delin, A. C. Fischer, S. Vaziri, F. Forsberg, M. Råsander, H. Hugosson, L. Bergqvist, S. Schröder, S. Kataria, M. Östling and M. C. Lemme, "Resistive Graphene Humidity Sensors with Rapid and Direct Electrical Readout", *Nanoscale*, vol. 7, pp. 19099–19109, Oct. 2015, DOI: 10.1039/C5NR06038A.

[30] A. Piazza, F. Giannazzo, G. Buscarino, G. Fisichella, A. La Magna, F. Roccaforte, M. Cannas, F. M. Gelardi and S. Agnello, "Effect of Air on Oxygen p–Doped Graphene on $SiO_2$", *Physica Status Solidi A*, vol. 213, pp. 2341-2344, Feb. 2016.

[31] Z. Cheng, Q. Zhou, C. Wang, Q. Li, C. Wang and Y. Fang, "Toward Intrinsic Graphene Surfaces: A Systematic Study on Thermal Annealing and Wet-Chemical Treatment of $SiO_2$–Supported Graphene Devices", *Nano Letters*, vol. 11, pp. 767–771, Jan. 2011, DOI: 10.1002/pssa.201532909.

[32] C. W. Jang, J. H. Kim, J. M. Kim, D. H. Shin, S. Kim and S.–H. Choi, "Rapid–Thermal–Annealing Surface Treatment for Restoring the Intrinsic Properties of Graphene Field–Effect Transistors", *Nanotechnology*, vol. 24, no. 40, p. 405301, Oct. 2013, DOI: 10.1088/0957-4484/24/40/405301.

[33] **E. J. H. Lee, K. Balasubramanian, R. T. Weitz, M. Burghard and K. Kern, "Contact and Edge Effects in Graphene Devices", *Nature Nanotechnology*, vol. 3, p. 486, Jun. 2008, DOI: 10.1038/nnano.2008.172.**

[34] **T. Mueller, F. Xia, M. Freitag, J. Tsang and Ph. Avouris, "Role of Contacts in Graphene Transistors: a Scanning Photocurrent Study", *Physical Review B*, vol. 79, p. 245430, Apr. 2009, DOI: 10.1103/PhysRevB.79.245430.**

[35] **A. Di Bartolomeo, F. Giubileo, S. Santandrea, F. Romeo, R. Citro, T. Schroeder and G. Lupina, "Charge Transfer and Partial Pinning at the Contacts as the Origin of a Double Dip in the Transfer Characteristics of Graphene–Based Field–Effect Transistors", *Nanotechnology*, vol. 22, no. 27, p. 275702, May 2011, DOI: 10.1088/0957-4484/22/27/275702.**

[36] **Z. Chen and J. Appenzeller, "Gate Modulation of Graphene Contacts – on the Scaling of Graphene FETs", *Symposium on VLSI Technology*, pp. 128–129, 2009.**

[37] **R. Nouchi and T. K. Tanigaki, "Charge-Density Depinning at Metal Contacts of Graphene Field–Effect Transistors", *Applied Physics Letters*, vol. 96, p. 253503, Jun. 2010, DOI: 10.1063/1.3456383.**

[38] T. Low, S. Hong, J. Appenzeller, S. Datta and M. S. Lundstrom, "Conductance Asymmetry of Graphene p–n Junction", *IEEE Transactions on Electron Devices*, vol. 56, no. 6, pp. 1292–1299, Jun. 2009, DOI: 10.1109/TED.2009.2017646.

[39] **B. Huard, J. A. Sulpizio, N. Stander, K. Todd, B. Yang and D. Goldhaber–Gordon, "Transport Measurements Across a Tunable Potential Barrier in Graphene", *Physical Review Letters*, vol. 98, p. 236803, Jun. 2007, DOI: 10.1103/PhysRevLett.98.236803.**